2017

# Technical Report

UNIVERSITY OF MARYLAND'S COLLEGIATE WIND COMPETITION TEAM


Andrew Dallas – Team Lead
Michael Queen – Electronics Lead
Andrew Jones – Aerodynamics Lead
Jason Cho – Mechanical Lead
Matt Blair – Testing Lead
Kevin Chung – Manufacturing Lead

**Dr. James Baeder –Principle Investigator**
**Dr. Vengalattore Nagaraj – Assistant Investigator**
**Mr. Marius Strom – Graduate Assistant**

# Table of Contents

Executive Summary ..... 2
Engineering Design ..... 3
Design Overview ..... 3
Turbine View and Specifications ..... 3
Turbine Configuration Selection ..... 3
Aerodynamics ..... 5
Blade Design ..... 5
Hub Design ..... 9
Annual Energy Production ..... 9
Yaw Design ..... 10
Mechanical Design ..... 12
Nacelle and Internal Components ..... 12
Brake System ..... 13
Nacelle Thrust Analysis ..... 14
Shaft Analysis ..... 14
Support Structure ..... 14
Electronics Analysis ..... 15
Turbine Electronics ..... 15
Load Electronics ..... 17
Generator ..... 17
Control ..... 18
Software ..... 19
Testing ..... 20
Blade Natural Frequency Tests ..... 20
Coefficient of Friction Tests ..... 21
System Parasitic and Cogging Torque ..... 21
Wind Tunnels Testing ..... 22
References ..... 24
Nomenclature ..... 24

## Executive Summary

TERPine Industries returns in 2017 with the MWT17, a turbine designed to maximize robustness and reliability. The MWT17 has been enhanced from the Diamondback (TERPine Industries' 2016 model), by including passive yaw, reducing part count, and improving efficiency in all wind regimes. The design team has taken the lessons learned from the Diamondback turbine and incorporated a variety of improvements in aspects of the turbine ranging from aerodynamics to the electronics. Extensive testing was conducted on the turbine to ensure its safety and efficiency.

The MWT17 is a traditional 3-bladed, upwind, horizontal-axis wind turbine with a direct drive connection to the generator. This configuration helps to provide a balance between efficiency and reliability and reduce the complexity of the design. The turbine prototype is rated for 23W at 2000 RPM with a cut-in speed of 3.2 m/s at standard sea-level conditions.

The blades have been designed to enhance both the peak power coefficient and the cut-in speed, allowing for more useful power at more wind speeds. New computerized tools were developed to optimize the aerodynamic design by testing a variety of different blade designs to make sure the MWT17's is the best.

*Figure 1: The MWT17*

The mechanical system has been a focus of the team. All physical components have been certified to be safe through experiment, analysis, and advanced computer design tools. Additionally, the brake system has been enhanced and now has over twice the braking power of the Diamondback Turbine. Many iterations and design improvements have been brought into this critical subsystem to make sure it is successful.

The electronics consume an ultralow amount of power, resulting in maximum usable energy production. A fast and efficient microcontroller runs safety and control algorithms to ensure that the turbine is responsive to dynamic wind speeds and regimes. New for this turbine, is a load with variable resistance, designed to match the power being produced by the turbine.

The whole turbine has also been packaged in a streamlined nacelle. The nacelle serves a practical purpose, to reduce drag and improve the flow to the tail vane. However, the new packaging also serves to increase the aesthetics of the turbine, making it an attractive symbol of renewable energy technology and deployable in a wider variety of environments.

Ultimately, the MWT17 is an efficient and robust turbine. The design team has used state-of-the-art analysis and incorporated features common to many modern full-scale turbines to make sure that this turbine is a viable clean energy solution. TERPine Industries is proud to present this efficient and competitive renewable energy device.

# Engineering Design

## Design Overview

*Turbine View and Specifications*

*Figure 2: Competition turbine CAD rendering (left) and implementation (right).*

| | **Test Turbine** |
|---|---|
| Configuration | Horizontal Axis Wind Turbine (HAWT) |
| Rated Power (sea level) | 30 W |
| Cut-in Speed (sea level) | 3.2 m/s |
| **Aerodynamic Specifications** | |
| Number of Blades | 3 |
| Blade Diameter | 0.45 m |
| Swept Area | 0.159 $m^2$ |
| Rated RPM | 2000 |
| **Structural Specifications** | |
| Tower System | Aluminum Monopole |
| Hub Height | 60 cm |
| **Mechanical Specifications** | |
| Braking System | Mechanical Friction Element Disc Brake |
| Braking Actuation | 2 x HS-81 Servos |
| **Electrical Specifications** | |
| Controller | TI MSP430 |
| Generator | Turnigy 3508 Gimbal Motor |
| Operating Voltage | 31.5 V |

*Table 1: Turbine Specifications.*

### Turbine Configuration Selection

The TERPine Industries engineering team began the wind turbine design process by determining the design objectives for the turbine. The team's focus was to improve on last year's performance and develop a robust turbine that is reliable in a variety of operating conditions.

| Criteria | Criteria Weight | HAWT (upwind) | HAWT (downwind) | DAWT | Darrieus | Drag Device | Cycloturbine |
|---|---|---|---|---|---|---|---|
| **Power Curve** | 5 | 0 | -7.5 | 5 | -10 | -15 | -10 |
| **Power/Speed Control-ability** | 3 | 0 | 0 | 0 | 0 | -3 | 0 |
| **Cut-in Speed** | 3 | 0 | -3 | 0 | 0 | 3 | 3 |
| **Durability** | 3 | 0 | 0 | -3 | 0 | 3 | -3 |
| **Manufacturability** | 4 | 0 | 4 | -4 | -4 | 4 | -8 |
| **Yaw performance** | 4 | 0 | 4 | -4 | 8 | 4 | -4 |
| **Safety** | 3 | 0 | 0 | 3 | 0 | 3 | 0 |
| **Appearance** | 2 | 0 | 0 | 0 | 2 | -2 | -2 |
| **Noise** | 2 | 0 | 0 | 0 | 2 | -2 | -2 |
| | **Configuration Totals:** | **0** | **-2.5** | **-3** | **-2** | **-5** | **-26** |

*Table 2: Pugh Matrix with weighted scores for various turbine configurations.*

The team began the configuration selection process by considering 6 potential turbine configurations: an upwind horizontal axis wind turbine (HAWT), a downwind HAWT, a diffuser augmented wind turbine (DAWT), a Darrieus vertical axis wind turbine, a drag-powered wind turbine, and a vertical axis cycloturbine. Using the HAWT as a baseline, each configuration was evaluated against 8 criteria using a Pugh matrix, shown in Table 2. The 8 criteria and their importance were derived both from the points allocated in the competition to performance criteria (e.g. power curve and cut-in speed) and evaluation of hallmarks of successful wind turbine design (e.g. ease of manufacturing and safety). The team assigned weights on a scale of 0 to 5 for each criterion for the competition turbine. Each configuration was then subjectively assigned a score between -3 to 3, with negative scores indicating the configuration is worse than the HAWT baseline and positive scores indicating the configuration is better than the baseline. Each score was multiplied by the weight of the category to determine the configuration's final score in each category. Configurations like the Darrieus and drag-powered device performed well in manufacturability and yaw performance, and configurations like the DAWT performed well in power production, but because of its balanced attributes, the standard upwind HAWT proved to be the superior configuration. This selection diverges from the Terpine Industries 2016 configuration of a DAWT, primarily because the addition of yaw requirements and relatively decreased competition weight of power production (as compared to cut in and controllability) reduced its Pugh matrix score. The spider chart shown in Figure 3 provides an overview of the scores and how each configuration was scored against the various criteria. From this chart, it is clearly seen that each of the configurations had at least one or two categories in which it performed much worse than the upwind HAWT design.

Several other configuration choices were made in support of our goals of reliability and simplicity. Using 3 blades was chosen because it provided a balance amongst cut-in torque, peak power coefficient, and manufacturability requirements. Based on results from further testing of the 2016 Diamondback Turbine, the turbine did not greatly benefit from a gear ratio other than 1:1, so this year's turbine was converted to direct drive[1]. Additionally, a fixed-pitch configuration was chosen for the blades to maintain simplicity. The low-cut in speed and braking afforded by variable-pitch mechanisms is compensated for by advanced blade design and a friction brake.

The wind turbine design was divided into the following subsections: aerodynamics (turbine blades and hub), structures and mechanics (nacelle layout, braking system, and tower), and electronics (microcontroller, power conversion electronics, generator, and sensing electronics).

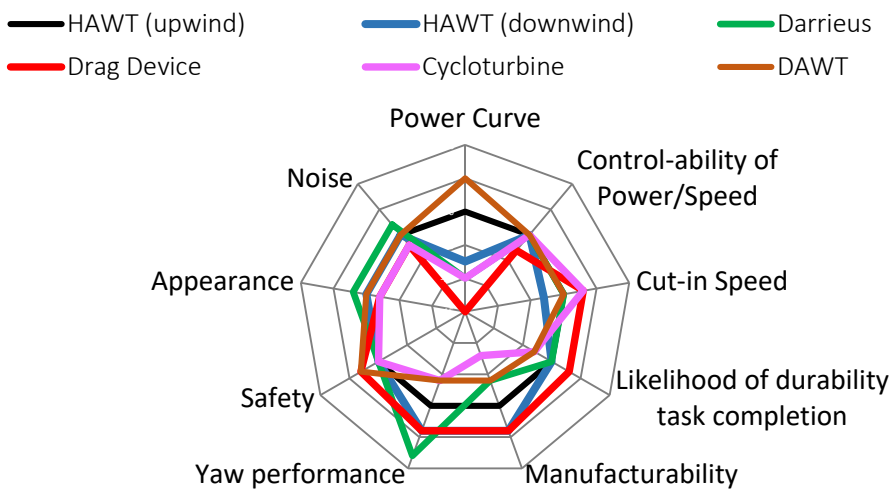


*Figure 3: Spider plot of the scoring of various configurations.*

**Aerodynamics**

The aerodynamics play a critical role in converting the energy of the wind into mechanical power. With the configuration of the 3-blade upwind HAWT chosen, the team needed to develop a set of efficient blades and hub system to safely and efficiently extract the wind's kinetic energy. The rotor and hub were designed using state of the art airfoils and computational optimization routines to ensure ideal efficiency and power conversion. From the aerodynamic design, the expected power of the turbine could be estimated, and the resulting loads on the rest of the turbine was determined.

*Blade Design*

The MWT17 turbine blades were designed to optimize power production and decrease cut-in speed. Five major design parameters were identified: blade diameter, blade airfoil, tip speed ratio, blade chord distribution, and blade twist distribution.

The blade's tip diameter was set at 45 cm, which was the maximum possible size within the competition constraints, to maximize capture area.

There were several considerations for the selection of the blade airfoil. The first objective was a high lift-to-drag ratio at the relatively low operating Reynolds numbers. Fulfilling this objective results in high airfoil efficiency, and as a result, high power generation. The second objective was that the airfoil has a relatively high peak lift coefficient. Higher lift coefficients were desirable primarily to provide more torque to decrease cut-in speeds. Finally, the airfoil had to be thick enough to provide structural stability to the blade.

The SG6043 airfoil was selected because it met this criterion the best. Other airfoils such as the Gottingen 79 and Eppler E63 were also considered and have better lift-to-drag performance than the SG6043, but displayed inferior peak lift coefficients or were too thin to hold the predicted stresses. Research done at the University of Maryland has shown benefits to using thin airfoils with sharp leading edges at low Reynolds numbers[2], but these airfoils were ruled out because manufacturing the precise edges of these airfoils at the test turbine's scale was infeasible. Using different airfoils at different radial

locations was considered, but since the SG6043 was analytically found to provide enough strength and had strong aerodynamic characteristics, it was used throughout the blade. The profile for the airfoil is shown in Figure 4.

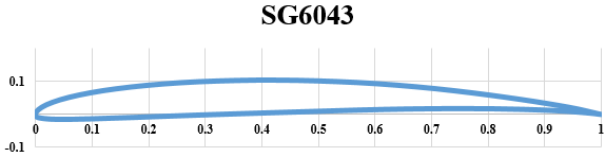


*Figure 4: Airfoil selected for rotor.*

The third design parameter, the tip speed ratio, was determined once the blade airfoils were selected. The SG6043 airfoil has a maximum Cl/Cd ratio of about 40 at an angle of attack of 9° at the operating Reynolds Number according to XFOIL simulations. Using this value, a design tip speed ratio of 4.61 was determined from analytical relations in Manwell et al. to provide the best power coefficient.[3] The team decided to design for a lower tip speed ratio of 4.0 to increase the blade torque at rest to achieve a lower cut-in speed and reduce the rotational inertia. This tip speed corresponds with a maximum RPM of 2000 at a wind speed of 11 m/s. At this tip speed ratio and wind speed of 11 m/s, the tip Reynolds number for a 2 cm blade in sea level density is 54,000. Since the turbine is designed to perform in Denver which has a density approximately equal to 0.96 kg/m$^3$, the Reynolds number is closer to 42,600.

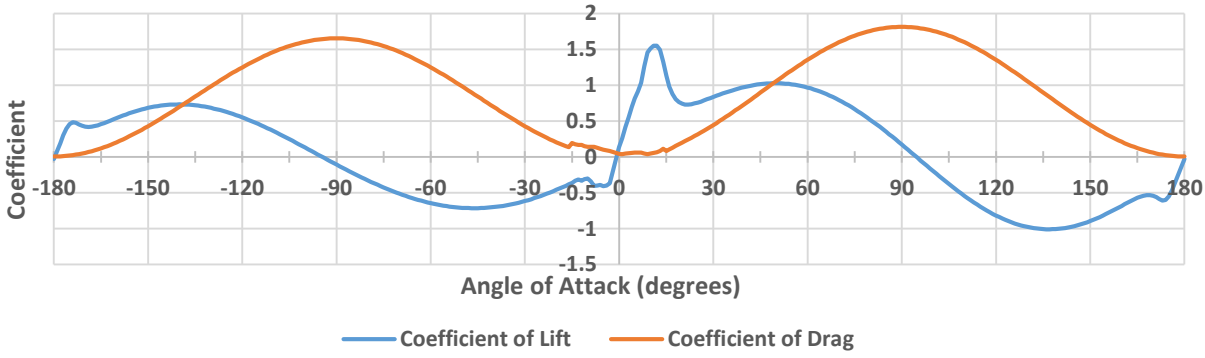


*Figure 5: 360° Lift and drag coefficent data.*

A blade element momentum theory (BEMT) program, with airfoil lookup, tip-loss, and axial and angular induction was developed to predict rotor performance. To build the airfoil lookup table, the SG6043 was simulated in XFOIL at a representative Reynolds number for angles of attack between -2 and 14 degrees, and the 360° polar was created in QBlade using the Mongtomerie model.[4]

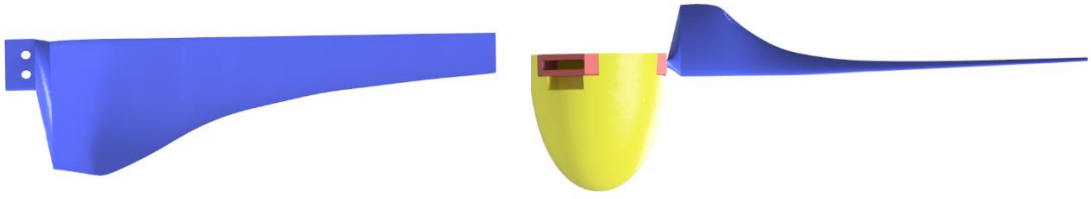

*(a) Blade planform* *(b) Blade attached to hub*

*Figure 6: CAD of final blade design.*

Using the airfoil and tip speed parameters, the Betz optimum twist and chord distribution was chosen as a starting point for the design. An optimization routine was used to modify the blade elements

closest to the root. The objective function was defined by the points that could be earned in competition from the turbine by extracting the coefficient of power and starting torque from the BEMT program. The points for the power curve task were calculated using the coefficient of power and assumed electrical losses to determine the power produced at each wind speed. The cut-in speed points were calculated by finding at what speed would the torque of the turbine exceed the measured cogging torque of the system. This speed was then translated into the points score, using a step function. Because of this routine, the elements closest to the root had their angle of twist increased and chord modified. After the routine, the chord of the blade element closest to the root was slightly decreased to make it more similar to the hub attachment. The final design is shown in Figure 6. The final twist and chord distributions are shown in Figure 7.

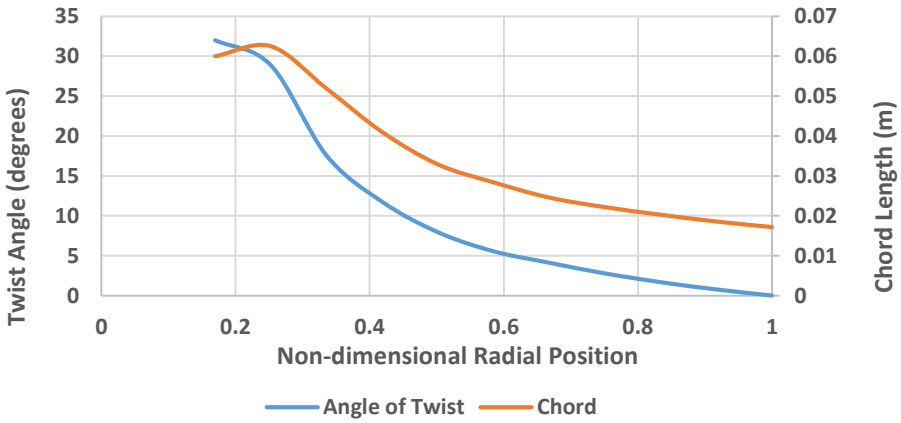


*Figure 7: Final blade parameters.*

Using the BEMT program, an aerodynamic $C_P$ (coefficient of power) and $C_T$ (coefficient of thrust) versus $\lambda$ (tip speed ratio) graph was generated and is shown in Figure 8. Note that the $C_P$ only represents the mechanical power produced by the rotor, and not the electrical power produced by the entire system, but the graph gives a general idea of the aerodynamic efficiency of the turbine and the power it can generate.

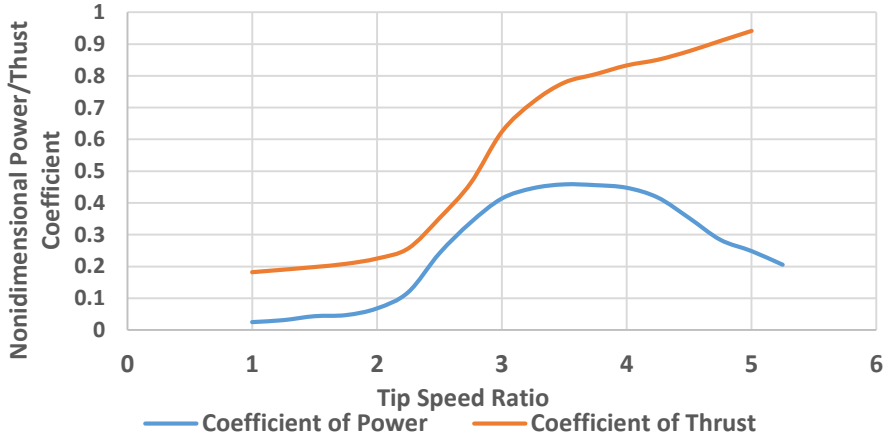


*Figure 8: Blade Element Momentum Theory predicted coefficient of power and coefficient of thrust.*

With this analysis, the turbine's peak coefficient of power was calculated to be 0.46. This is a reasonable value considering the tip speed ratio and low Reynolds number. In addition, the cut-in speed in Denver's typical air density of 0.96 kg/m$^3$ was calculated to be 3.7 m/s. This cut-in speed is 0.5 m/s lower than if the Betz optimum blades. The coefficient of power of the optimized blades is slightly lower than the Betz optimum blades as well, but the gain in cut-in performance should result in a net gain of points. Using the peak aerodynamic efficiency, estimated electrical losses of 50%, and the cut-in speed, the expected power output in Denver is shown in Figure 9. From the power calculations, the rated power of the turbine is 23 W in Denver, and 30 W at sea level.

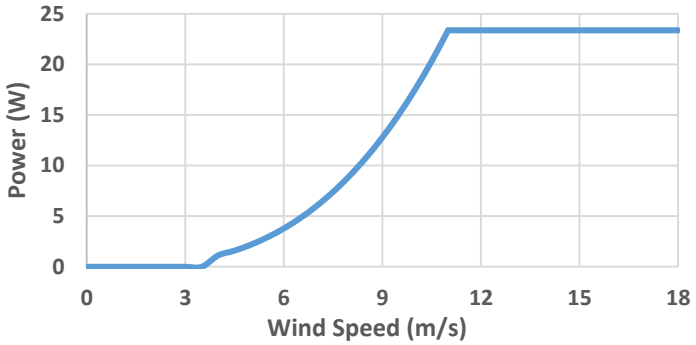


*Figure 9: Predicted power curve for the deployed turbine.*

The maximum possible thrust generated by the rotor was estimated by the following equation:

$$T = \frac{1}{2} C_T \rho U^2 \pi R^2$$

To provide an upper bound on the thrust, a value of 0.85 for the coefficient of thrust (which corresponds to the value at the design tip speed ratio), sea level air density, and a maximum wind speed of 18 m/s was used. This highest potential thrust was calculated to be 26.8 N. At 18 m/s, the turbine should be operating at a lower tip speed, and a lower $C_T$ as a result, but this overestimate was used to ensure the safety of the design of the nacelle and support structure.

The blades are manufactured using the SLA method of 3D printing. This manufacturing method allows for precise shapes, and a smooth, aerodynamic finish. The printing material is VeroBlack, a similar material to Nylon, and have a modulus of elasticity of 2.2 GPa and tensile strength of 50 MPa.[5]

The largest loading the blades will experience is due to the centrifugal loads at the peak rotational speed. Due to the complexity of the geometry, the blades were simulated with Autodesk Inventor's finite element analysis package. When simulated with a centrifugal load equivalent to that experienced at 4000 RPM, twice the rated rotational speed, the blades still had a safety factor of 2.1 with most of the stress occurring near the root. Based on this analysis, this blade design was determined to be safe for operation.

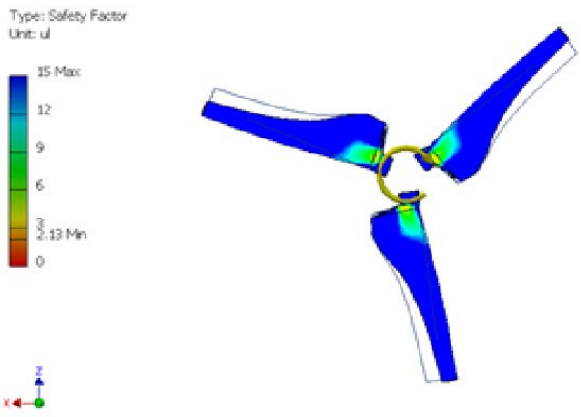


*Figure 10: Finite element analysis results of the rotor blades.*

*Hub Design*

The main objectives for the hub design were to develop a way to hold the blades securely and minimize the drag force on the turbine. The hub was 3D printed in two separate pieces, the base and the nose cone, shown in Figure 11. They were printed separately so that the nose could be manufactured hollow to reduce the moment of inertia about the drive shaft, and the base was manufactured solid to provide additional strength. The nose cone was designed to follow the profile of a NACA0030 airfoil, to streamline the flow around the turbine. The two pieces press fit together after printing. The blades are secured to the base by two bolts that pass through matching holes on the blades and are tightened with nuts.

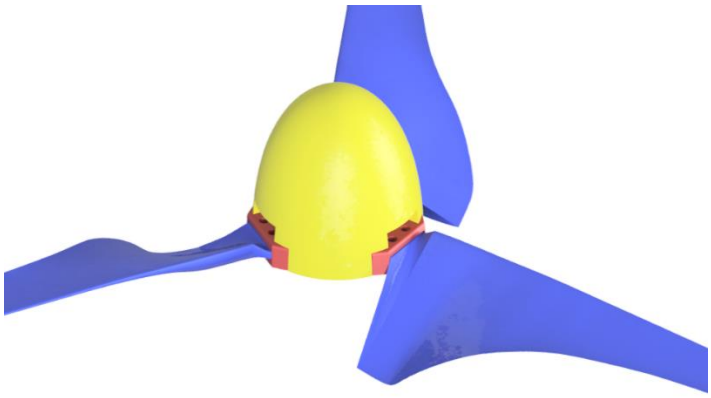

*Figure 11: Close-up of the hub base (red) and the nose cone (yellow).*

*Annual Energy Production*

The turbine was scaled to a 5m diameter to estimate how a more realistic small turbine based on the MWT17 design would perform in the real world. The aerodynamic coefficients and electrical efficiency are assumed to stay the same. It is important to note that the larger turbine would be operating at higher Reynolds Numbers than the test turbine, thus viscous drag would be relatively lower and the airfoils would have improved lift-to-drag, so it is likely that the coefficient of power for the larger turbine would be even higher. The two diverse locations of Denver, CO and College Park, MD were used to judge performance for varying average wind speeds and power densities.

The average wind speeds for areas near the chosen locations at an 80m hub height were found using NREL's Wind Prospector tool.[6] To estimate the wind speed at a more realistic 20m hub height for small turbines, the wind profile power law equation below was used. From this process, it was determined the average wind speed the turbine would see at a 20m hub height was 5.7 m/s in Denver, and 4.1 m/s in College Park.

$$U = U_r \left(\frac{z}{z_r}\right)^{0.143}$$

From the average wind speed, a Rayleigh distribution of the wind was produced and can be seen in blue in Figure 12. The power from the turbine was calculated based on the local air density, cut-in speed, coefficient of power, and electronics efficiency. The power produced at different wind speeds is also plotted in Figure 12 in orange. Since the density is higher in College Park, the power produced is higher and the cut-in speed is lower in that location.

The power weighted by its probability was then integrated to give an average power production. From this integration, it was found that on average, the turbine in Colorado would produce an average of 665 W/hr for an annual production of 5,830 kW-hr. This amount of power would be able to account for most of a household's energy production. Despite the higher density in College Park leading to higher

potential power at a given wind speed, the lower average wind speed means it would only average 339 W/hr for an annual production of 2,970 kW-hr.

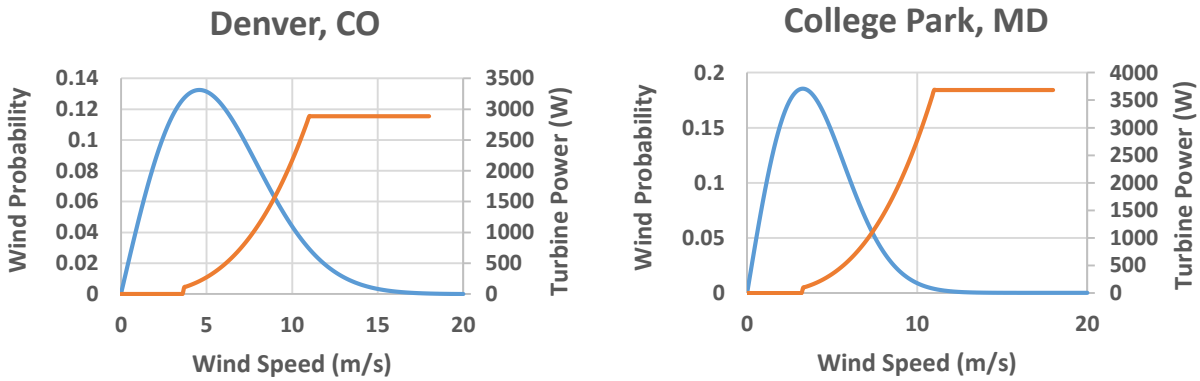


*Figure 12: Wind speed probabilities and turbine power productions as a function of wind speed in differing locations. The blue line signifies the wind probability distribution, and the orange signifies the power production.*

**Yaw Design**

New for this year, the turbine was designed to enable yawing moments with respect to the wind turbine's support structure. This new objective required a restoring moment to the turbine such that wind that is blown at an angle relative to the orientation of the wind turbine will not affect its performance. For the MWT17 design, a passive tail was used to create a restoring "lift" force that cancels any disturbing moment developed by a change in the freestream direction.

The tail stands 16 inches in height, with a semi-circular planform. A gap in the middle is included to allow the nacelle fuselage to fit in, providing the maximal planform area. The tail is designed so that it is at its tallest as far back as possible, to increase the size of lift force's moment arm and resulting restoring moment. A CAD render of the turbine tail can be seen in Figure 13. The tail was simply cut from a sheet of ABS plastic.



*Figure 13: Planform view of tail.*

To allow for the freedom to yaw, two shaft collars are fastened to the support shaft. These shaft collars constrain the nacelle base between two bearings so that the nacelle can move in the yaw direction, but not in the remaining 3 translational or 2 rotational directions. The thrust of the rotor does cause some minor friction with the nacelle base plate and the support tower which was found to not impede the yawing of turbine and helps to provide some damping to the yaw motion. Since the turbine is only required to make 2 complete revolutions, a slip-ring was considered to allow the wires to move more freely through the turbine, but ultimately deemed not necessary for the test turbine. The shaft collar and bearing configuration can be seen in Figure 14.

With the constraints on the motion provided by the yaw bearing configuration, the overall motion of the wind turbine can be represented as a one degree of freedom problem. The turbine is treated as a rigid body and the tail is approximated as a flat plate for analysis. Additionally, the rotor thrust was simplified into contributing a point force in the direction of the freestream velocity at the center of the rotor. With these simplifications, the following equations describe the behavior the turbine in yaw.

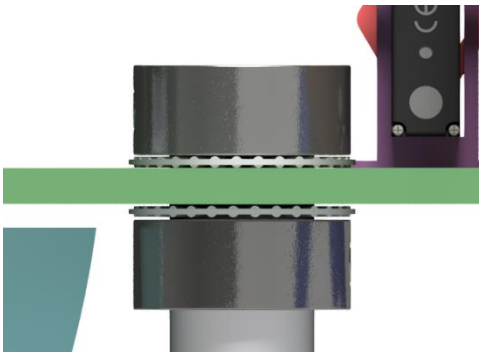

*Figure 14: The turbine's yaw bearing configuration.*

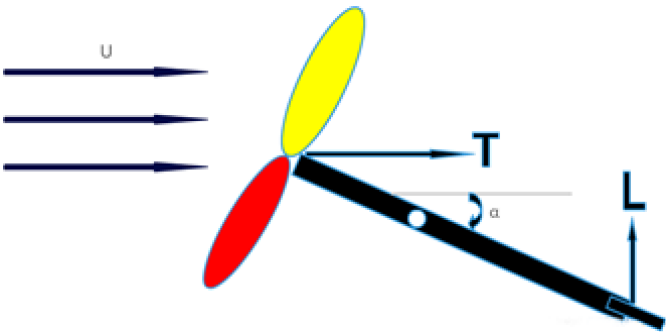


$$M_G = I_G \ddot{\alpha}$$

$$L = \frac{1}{2} c_L \rho_\infty u_\infty^2 S$$

$$c_L \approx 2\pi\alpha$$

$$T = \frac{1}{2} C_T \rho_\infty u_\infty^2 \pi R^2$$

*Figure 15: Overhead Free-Body Diagram of turbine (left) and governing equations for tail (right).*

A Free-Body Diagram of the turbine's forces acting to yaw the turbine can be seen in Figure 15. By summing the forces on the turbine, and having the restoring "lift" force to act at the center of pressure of the tail vane, the governing equation for the angle of attack of the tail relative to the freestream is:

$$\ddot{\alpha} = \frac{l_2 \cos(\alpha)\, L - l_1 \sin(\alpha)\, T}{I_G} - \zeta \dot{\alpha}$$

The variables $l_1$ and $l_2$ are the lengths along the turbine from the tail and blades to the turbine's center of rotation, respectively, and $\zeta$ is an assumed frictional damping constant of 6 $s^{-1}$. By putting this equation into MATLAB for further analysis of the turbine's movement, it was determined that regardless of the initial angle of attack of the turbine within the small angle approximation, the turbine will return to parallel with the freestream within a few second timespan. The damping constant and simulation were validated against wind tunnel tests. An example of the results of a MATLAB simulation can be seen in Figure 16.

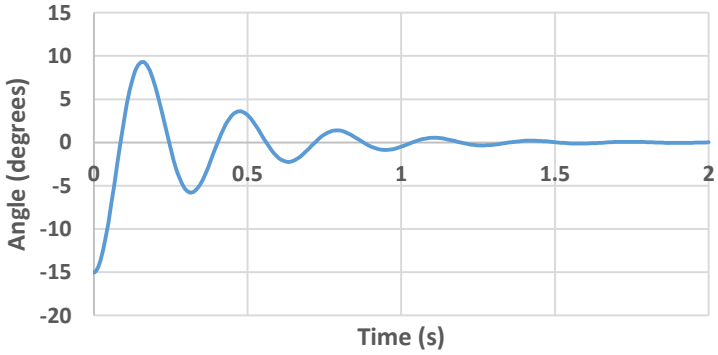


*Figure 16: MATLAB simulation of tail movement, initially perturbed at angle of 15 degrees.*

**Mechanical Design**

The mechanical subsystem is integral to both the power production and safety requirements of the test turbine. More specifically, these subsystems facilitate the conversion of kinetic rotational energy to electrical energy, allow the maintenance of a safe rotational speed, and enable turbine shutdown. Design decisions involving the mechanical subsystem of the prototype turbine are guided by the following: safety and durability, wind tunnel and test section space restrictions, and shutdown requirements. Subassemblies and functions deemed necessary to meet these requirements are as follow:

- Nacelle housing: connects to the tower and protects the mechanical and electrical components of the turbine
- Drive train: provides transmission of the rotor to the generator for power production
- Braking mechanism: responds to the microcontroller's commands and safely brakes the turbine when necessary

*Nacelle and Internal Components*

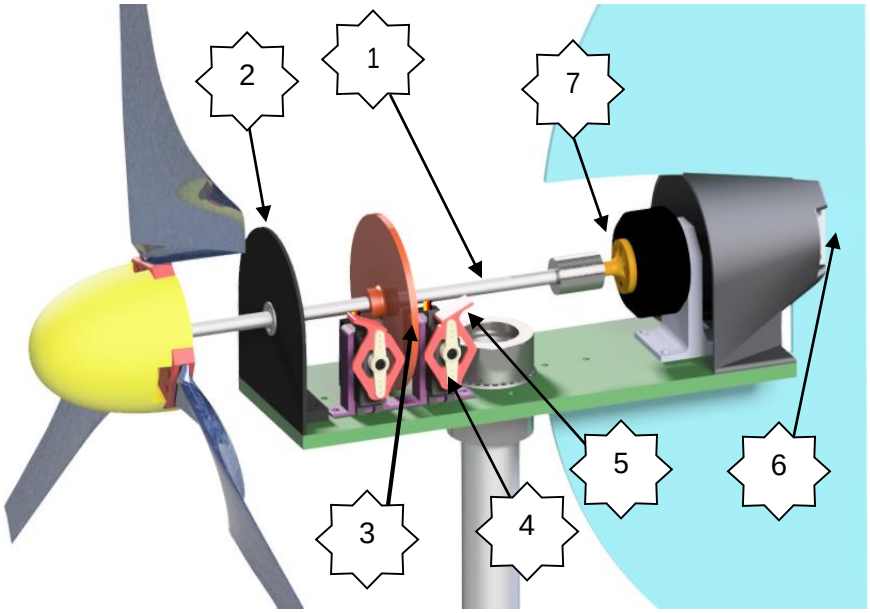


*Figure 17: Uncovered nacelle design and component layout.*

The nacelle layout is shown in Figure 17. The unique configuration is designed to position the braking mechanism in close proximity to the shaft and to balance the center of gravity of the turbine around the center of rotation. Depicted in Figure 17 are the following components of the competition turbine and their corresponding functions:

1. Rotor shaft: connects the turbine rotor to the generator, and braking mechanism
2. Nacelle Front Wall: protects components and resists the thrusting force of the rotor blades
3. Brake disk: provides a contact surface on the shaft for the braking mechanism
4. Brake servo: actuates the brake arm in response to voltage detection system
5. Brake arm: provides a resistive friction force that brakes the turbine
6. Tail fin: facilitates the yawing of the nacelle into the direction of the wind
7. Generator: gimbal motor converts the rotational energy of the shaft to electrical energy

*Brake System*

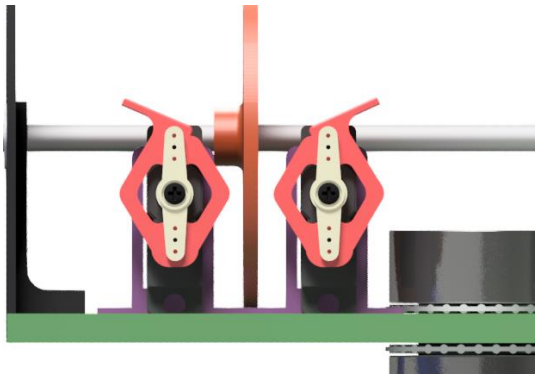

*Figure 18: Braking mechanism.*

When designing the brake system, the main criteria were effectiveness, simplicity, and space constraints. A servo motor system was chosen over a hydraulic or linear actuating system because not only are actuators available in the required size, but they also cut down on the complexity and the number of additional parts that needed to be designed. Instead of using an RPM sensor to detect when to activate the braking system, an electronic sensor was used that utilizes a scaled down unregulated voltage reading, and the linear relation between voltage and RPM to establish a braking cut off point. Two servos, one from each side, are used to clamp the brake disk to reduce bending of the brake disk and double the effective normal force and thus double the frictional force/braking torque.

The actuator uses its torque, represented by the green arrow in Figure 19, to enact a normal force on the brake disk. This normal force, represented by the pink arrow, is calculated from the servo specifications and brake arm geometry to be 25.5 N. The resulting frictional force applied to the brake disk can then be found by multiplying the normal force from the servos by the coefficient of friction. The coefficient of friction was experimentally determined to be 0.8 using the procedure detailed in the Testing section, resulting in a frictional force of 20.4 N on the brake disk. This frictional force causes the braking moment, shown in blue. Since this force is applied 3.0 cm from the center of rotation, the braking torque is ultimately 0.612 Nm.

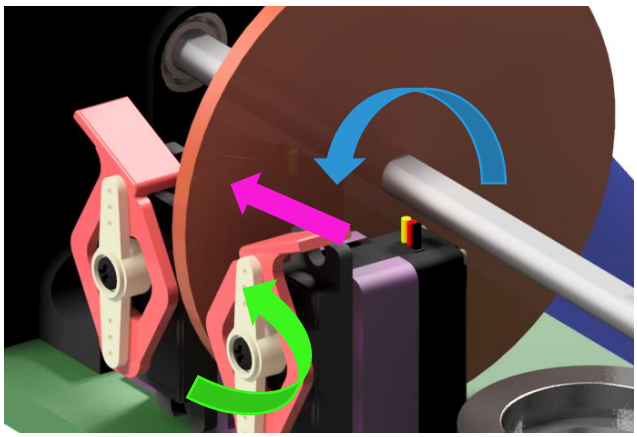

*Figure 19: The servo moment in green causes a normal force in red on the brake disk. This normal force results in a frictional breaking moment about the shaft shown in blue.*

To calculate the time to stop, the moment applied from one servo is doubled to account for both servos. The equation below relating the braking moment, rotational mass moment of inertia, and the

angular acceleration required to stop the brake disk was used. Since the brake should be effective in emergencies, a worst-case rotational speed of 4000 RPM was used. The mass moment of inertia for the rotational system was determined in Autodesk Inventor to be .00771 kg*m$^2$. The resulting time to stop was calculated to be 2.64 s, and from this analysis, it is clear the turbine can break within the required competition time.

$$\Delta t = I_m \frac{\Delta \omega}{\tau}$$

*Nacelle Thrust Analysis*

Two components, the motor mount and the front wall, act to resist the force of thrust from the rotor. Each component was designed to individually resist the peak thrust of 26.8 N to account for the worst case in which the other failed to carry any of the load, and were 3D printed in ABS. Using Autodesk Inventor's finite element analysis, a force was simulated at the center of the circle of 26.8 N. This analysis allowed a parametric study of component thicknesses and resulted in the current design. The minimum safety factor of the final design of front wall was determined to be 2.86 and the minimum safety factor of the motor mount was determined to be 8.95. As a result, these components are expected to remain sturdy and safe throughout operation. The results of the finite element analysis can be seen in Figure 20.

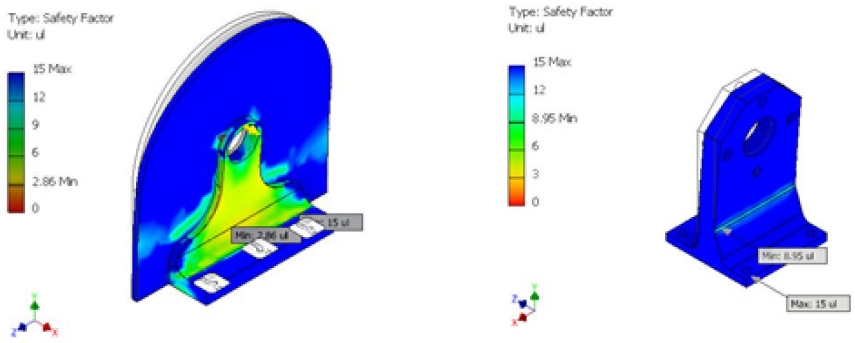


*(a) Front wall* *(b) Motor mount*

*Figure 20: FEA results of the thrust bearing components.*

*Shaft Analysis*

The shaft must withstand repeated stresses over its lifetime associated with starting and stopping the rotor. At the rated wind speed of 11 m/s, the rotor produces a mechanical power output (before electrical losses) of 60 W at 2000 RPM. The shaft is made from 303 Stainless Steel with an endurance strength of 240 MPa and has a radius of .003175 m.[7] From the equations below, a torque of 0.285 Nm, shear stress of 5.71 MPa, and a resulting safety factor of 41.8 can be calculated. This analysis shows that the shaft has an incredibly low likelihood of ever failing due to fatigue, and since the endurance strength is lower than the yield strength, the safety factor for yield is even higher.

$$T = \frac{P}{\omega} \quad J = \frac{\pi R^4}{2} \quad \tau = \frac{Tr}{J}$$

*Support Structure*

The structure of the competition turbine serves as an interface for the competition wind tunnel and the power generation components of the turbine. The initial sizing of the turbine structure and

baseplate was determined based on the test wind tunnel constraints. The baseplate and connection to the tower can be seen in Figure 21.

Aluminum 6061 was chosen as the primary material for the tower because it has a favorable strength to weight ratio and is easy to work with. A hollow aluminum tube with an outer diameter of 2.54 cm was used because it both satisfied the minimum calculated diameter necessary for structural soundness, and provided a way for the power wires to run down the length of the tower.

The primary design loads experienced by the tower can be broken into two main categories: steady loads and dynamic loads. The main steady loads on the structure were the rotor thrust and the weight of the rotor and nacelle components. The dynamic loads encompassed turbulence, cyclic loads, start/stop impulsive loads, and resonance-induced loads. Resonance-induced loads were used primarily for design since the order loads are on a much lower order of magnitude.

The steady loads, namely normal stress on the tower, was calculated using a length of 60 cm, a moment of inertia of $1.39*10^{-8}$ $m^4$, and a nacelle weight of 0.83 kg. Max thrust on the tower was calculated to be 26.8 N in the Aerodynamic Section. The calculations for peak normal stress on the tower was determined with the equation:

$$\sigma = \frac{Mr}{I} + \frac{mg}{A}$$

The max stress was calculated to be 14.7 MPa. The yield stress for Aluminum 6061 is 276 MPa[8], resulting in a Safety Factor of 19.

To analyze the vibration characteristics of the structure, the tower and nacelle was modeled as a vertical cantilever beam fixed at one end and free at the other. A calculation of the natural frequency of the tower was determined with the equation:

$$\omega = \sqrt{\frac{3EI}{mz^3}}$$

The natural frequency of the tower was found to be 127 rad/s, equivalent to 1210 RPM. The turbine passes through this natural frequency on its way to the rated rotational speed. The tower design ensures that it does not coincide with the rotor excitation frequency or the blade pass excitation frequency, so that additional resonance does not occur.

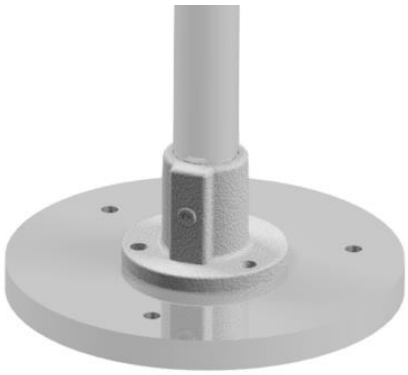

*Figure 21: CAD drawing of the baseplate connection and tower.*

**Electronics Analysis**

The turbine electrical system serves two purposes. The first challenge for the electronics is to condition the output of the generator to form useable power. The second is to interface the software control strategy to the hardware. Efficiency was the primary guiding principle for the design of this subsystem, and reducing the power usage of the control electronics was a priority. The electronics schematic which resulted from the design can be seen in Figure 22.

*Turbine Electronics*

Power conversion is performed passively with a 3-phase rectifier. The output voltage of the turbine varies from 0 to 30 volts depending on the output power level. The output voltage is not regulated to a single value so that there are no additional losses on the turbine side. Once output voltage exceeds approximately 4.75 volts, a buck converter steps down the voltage internally for use by the control

electronics to 3.3V. A buck converter was chosen as opposed to other regulators such as linear or Zener regulators because of its high efficiency. At the operating voltage, the Hall Effect sensor operates with 91% conversion efficiency. A boost converter could potentially be used to power the control electronics when the output is at a lower voltage, but in that region the power generated is insufficient to power the electronics.

The microcontroller used is the Texas Instruments (TI) MSP430 Launchpad. This microcontroller was selected because of the documentation and support for TI microcontrollers, low power consumption, and sufficient number of input and output channels. The Launchpad operates at lower power than comparable Arduino microcontrollers that operate at 16 Hz, enabling fast, low-power performance.

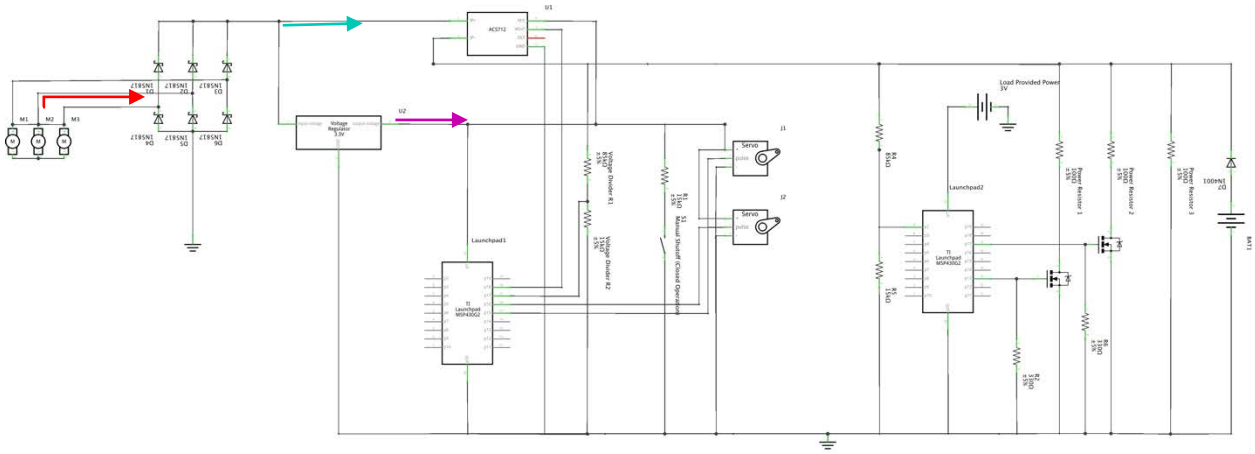

*Figure 22: Test turbine electronics schematic. The red arrow represents three-phase AC power, the light blue represents unregulated DC power, and the magenta represents regulated 3.3V.*

The electronics utilize three different sensors to monitor RPM, current produced, and the shutoff condition. The simplest sensor, the shutoff switch is simply a normally closed switch with a pull-up resistor which is monitored by the microcontroller. This solution provides robust and low power operation. Current production is sensed with a Hall Effect current sensor. A Hall Effect sensor is used because it is efficient and draws little current. The current sensor is used to both monitor if the load is connected and how much current is produced. The final sensor is the voltage divider sensor. There are several options for measuring RPM, but the voltage divider requires essentially no power to operate because of the high values of the resistors used and has fewer parts in the turbine, increasing reliability and efficiency. This system allows the MSP430 to monitor the voltage being produced, from which the microcontroller can infer the turbine rotational speed.

Actuation is performed with dual servos for the mechanical braking mechanism. The mechanical brake consumes the most power of the system when in operation at slightly more than 1 Watt. Fortunately, the brake will only be in operation when the system is producing a significant amount of power, so the brake will not decrease power produced by a significant percentage in the power curve region.

Power consumption calculations estimate that the control electronics will draw just above 1 Watt in the worst case scenario as indicated in Table 3. This power consumption is 8% of the rated power found from wind tunnel testing. Electrical tests done on individual components indicate that 1.65W is a reasonable upper bound on power consumption because this is only in the worst case scenario where the braking mechanism requires 95% of the power being consumed. This case is also only in effect when the power should be diverted to braking, and not during the power curve. In normal operation, the brakes are not active so their idle current draw is only 8mA giving an idle power consumption of 26.4 mW, 81% less than in the worst case scenario.

| Component | Voltage (V) | Current (mA) | Power Consumption (mW) |
|---|---|---|---|
| MSP430 | 3.3 | 11 | 36 |
| RPM Voltage Divider | 30 | 2 | 60 |
| Servo (HS-81) (for both) | 3.3 | 420 | 1,380 |
| Manual Shutoff | 3.3 | 10 | 33 |
| | | **Total:** | **1,510 (1,650 after DC converter losses)** |

*Table 3: Worst case power consumption for main power consuming parts.*

*Load Electronics*

For the competition, the load is represented by a set of power resistors. Resistors were chosen for the load because it would limit the impact of the load on the performance of the turbine. Inductive loads like that of a motor would have a resonant effect on the turbines. It was found that higher resistance improved power production, but since the turbine had to be kept under a voltage of 36 V to avoid damaging components, additional power resistors on the load are activated in parallel to increase the current and decrease voltage. These power resistors are activated digitally at a threshold of 22V through an NPN-MOSFET gate to increase the load resistance as power is increased, and deactivated at a threshold of 10V. This strategy allows better matching of the power generation to the resistance required.

*Generator*

Selection of the generator proved to be one of the most critical components of the design. In order to enhance performance in the competition, the primary goals of the generator were to maximize energy production efficiency and minimize cogging and parasitic torque.

Generators can be divided into two categories: synchronous and asynchronous. As the turbine is tested off-grid, the synchronous, or induction, generators would not work as they are dependent on a grid to provide a slip frequency. Additionally, these generators rely on excitation current at startup. Asynchronous, permanent magnet generators do not suffer from these disadvantages and they perform well in a wide variety of operating conditions.

Unfortunately, power generation and cogging torque data for generators at the scale of the competition turbine (below 50W), is not easily found. To make an informed choice on an appropriate generator, testing to characterize the performance of a variety of generators needed to be done.

Several motors were tested by driving them at a rotational speed typical of the turbine. The generators were connected to a 3-phase rectifier and the power across a load resistor was measured. The motor parameter which had the most influence on the power production was the kv rating. Figure 23 shows the variation of power production with kv rating. Based on these results, lower kv ratings are clearly ideal for power generation in the RPM range that is expected.

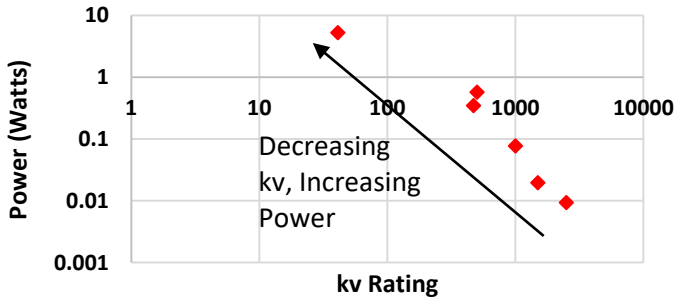


*Figure 23: Generator power production vs. kv rating for a variety of Turnigy and Quantum branded BLDC motors.*

Cogging torque was also an important criterion for selecting the generator. A simple static torque measuring setup was developed to determine the cogging torque, similar to how the whole system's parasitic and cogging torque was measured. A level lever arm was attached to the generator and loaded with weights until it began to rotate. From this, the torque required to start the generator was calculated.

**Control**

Traditional turbine control is typically achieved through three methods: yaw control, rotor rotational speed control, and pitch control. Directional yaw for this turbine is provided via a passive yaw mechanism, so active yaw control was not used. Additionally, since active pitching control adds a significant amount of additional components and would negatively impact reliability, it was not used for the test turbine. Only active breaking for rotational speed control is implemented on the turbine.

The turbine operates in five distinct regions as shown in Figure 24. The regions are as follows:

I – Idle (Below 3.7 m/s): No rotation due to low wind speeds.

II – Startup (3.7 – 5 m/s): The turbine begins producing power, but exhibits no active control or sensing.

III - Power Curve (5 – 11 m/s): As the turbine begins producing enough power to support the electronics, it begins sensing to ensuring rotational speed does not exceed that of the rated speed.

IV - Constant Rotational Speed (11 – 18 m/s): The turbine uses a proportional control strategy to maintain constant rotational speed.

V - Shutdown: The turbine transitions upon activation of automatic shutdown or loss of load until it returns to idle.

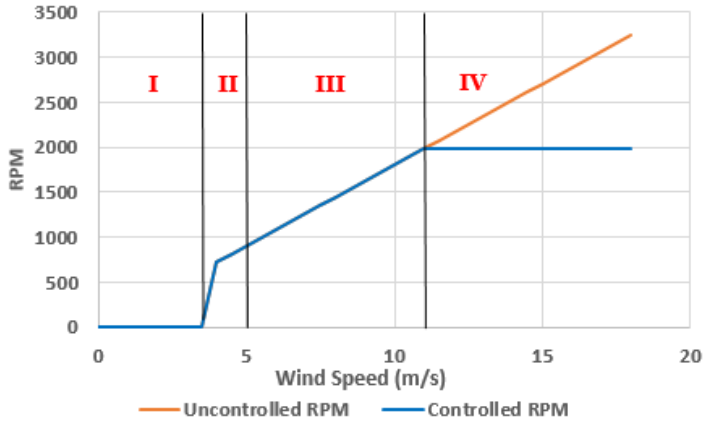


*Figure 24: Designed control regions. Note that Region V is not pictured as it is a transition region.*

The turbine subject to a constant input is a stable system as long as it is not operating at a natural frequency. As a result, the controller in Region IV can be implemented with a relatively simple system. An algorithm in which the force applied by the servo is proportional to the rotational speed above the rated speed is used for this region.

**Software**

The software design is meant to first prioritize response to urgent safety events, such as shutdown. The software's second priority is to maintain the turbine within its safe operating range. By focusing on these two priorities, the software can be kept as simple as possible to eliminate potential bugs. The Region III/IV control loop begins only after the turbine produces enough power to activate the microcontroller. The flowchart in Figure 25 is used to illustrate the decision making process of the software. Since responding to the shutdown requires quick response, the shutdown conditions are checked at the beginning of each control loop. Once either of these conditions is detected, the program enters shutdown mode. The shutdown also cuts off its power, but since the servo torque is reduced once the power is turned off, the turbine should not have any issues restarting. The servo brakes are also used to keep the speed and power at the rated conditions.

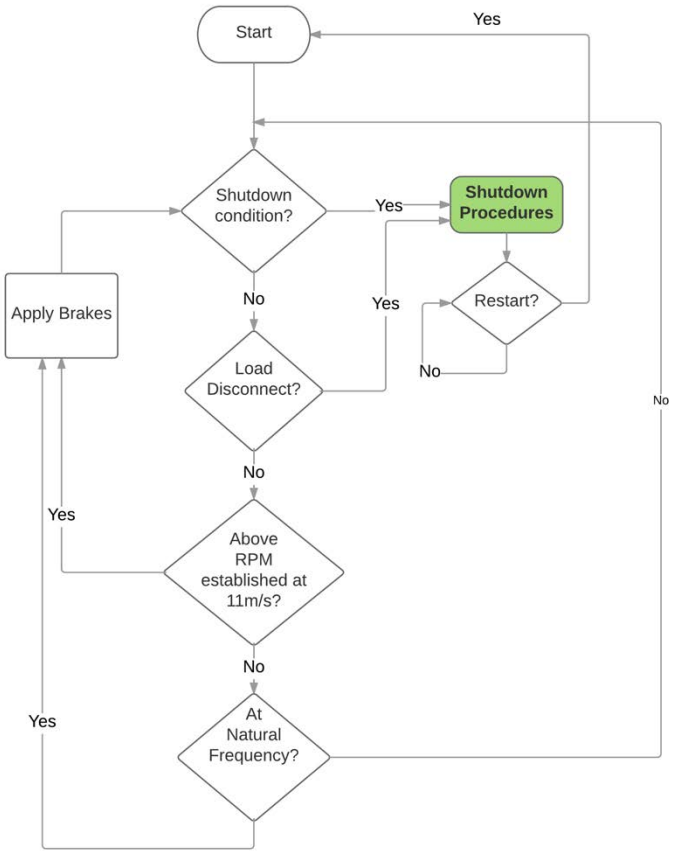


*Figure 25: The software logic.*

The software component of the microcontroller is focused on monitoring the power production of the turbine and managing shutdown. The MSP430 microcontroller is programmed through TI's Energia development environment which is a derivative of C++ and very similar to Arduino's development environment. There are many embedded libraries in the development environment available for controlling servos and measuring voltages which allow for effective control of the turbine.

On the turbine side of the circuit, the Hall Effect current sensor is connected to monitor the power being produced and determine when the turbine needs to be shut down in the event of a load disconnect. This sensor measures the current passing through and outputs a corresponding voltage that is read by the turbine microcontroller. The RPM is managed through measuring the linear relationship between voltage and RPM. The voltage is scaled down to 8% of its original value to be in the operating region of the MSP430. When the voltage is above our threshold voltage we determined for 11m/s RPM, the controller activates the brakes on the turbine. The voltage is calculated over an averaged sample to reduce noise and ensure it is truly in a shutdown condition state. The third connection to the turbine controller is the manual shutdown switch. In normal operation this is a closed circuit, and when it is disconnected the MSP430 will read a change in voltage signaling another shutdown condition.

**Testing**

*Blade Natural Frequency Tests*

The blade was tested for its natural frequency to ensure that the rotational speed would not excite any major vibrational modes. To measure the blade's dynamic response, a piezoelectric material was bonded to the blade, as shown in Figure 26.a. The piezoelectric material produces current when it experiences a deformation. This current is proportional to the amount of deformation, but is very small, so the current was fed through an amplifier circuit to produce a voltage signal, shown in Figure 26.b. After the signal was conditioned through the circuit, it was transmitted through a data acquisition system to a computer.


*(a) Piezoelectric bonded to blade* *(b) Amplifier circuit*

*Figure 26: The natural frequency test.*

The data acquisition system captured several time histories of the response of the blade to a tip impulse force when the blade was clamped at the root. One of the signals captured is plotted in Figure 27.a. Using the logarithmic decrement to determine the amplitude decay, the structural damping ratio of the blade is calculated to be 0.053. This value is higher than that of metal structures meaning the composite blades are better at damping out unsteady forces. By applying a Fourier Transform to the data, the time histories were transformed into a set of frequencies. These frequencies and their magnitudes are plotted in Figure 27.b. From this plot, it was determined that the first natural frequency is 43 Hz, and the second natural frequency is 119 Hz. The first natural frequency coincides with a rotational speed of 2600 RPM, well above the operating range of the turbine, so the turbine should not excite a resonant response in the blades.

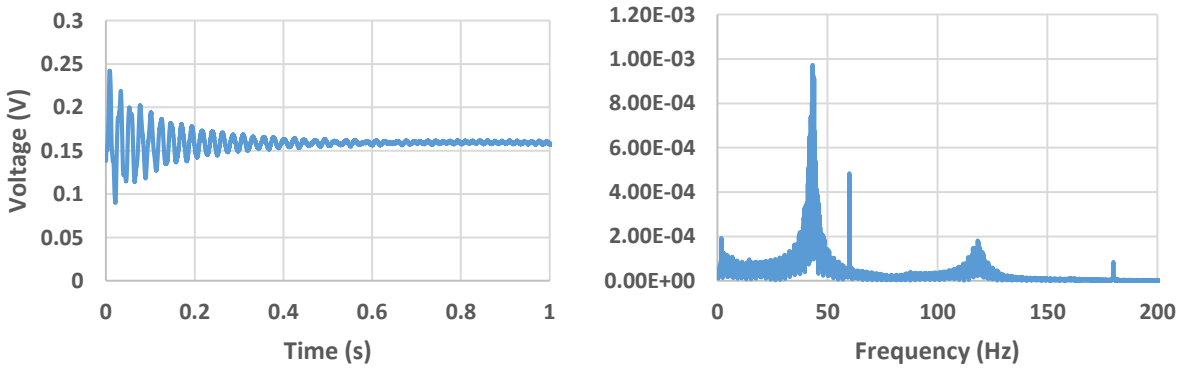


*(a) Impulse response* *(b) Fourier transform results*

*Figure 27: Data generated from blade tests.*

*Coefficient of Friction Tests*

To calculate the frictional force acting on the brake disk, the coefficient of friction between the two brake pads needed to be determined. First, the spring constant of a spring was determined using a known weight of 100 g. The unstretched length of the spring was compared to the length when a 100 g weight was attached to calculate this constant. The test setup can be seen in Figure 28.a.

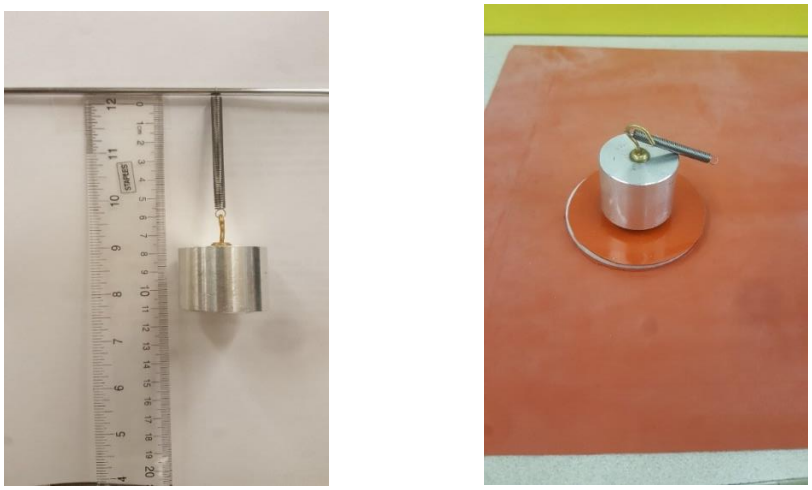

*(a) Characterization of spring* *(b) Characterization of rubber*

*Figure 28: Test setups to determine the brake material coefficient of friction.*

With the spring constant known, the brake disk was placed on a bed of the rubber material with the weight of 100 g on top to act as a known normal force. This setup is shown in Figure 28.b. The spring was then subject to an increasing horizontal input force, and the elongated distance of the spring once the disk started to move was measured. At that displacement, the force could be calculated using the spring constant, and used to solve for the coefficient of friction using the equations below. From this procedure, a coefficient of friction of 0.81 was found.

$$F = k\Delta x \qquad \mu = \frac{F}{N}$$

*System Parasitic and Cogging Torque*

To estimate the wind speed that would produce enough torque from the rotor to begin rotation, the parasitic and cogging torque for the bearings and generator needed to be determined. The nacelle and its components were installed as they would be during power production. However, instead of the rotor, a lever arm was attached to the power transmission shaft. A set of weights was added to the shaft. Weights were gradually added to the lever arm until the shaft began to turn. From the weight applied and the length of the lever arm, the torque required to turn the shaft could be calculated. For the MWT17, this turned out to be 6.56 mN. This data was then used to determine starting speed. This test setup can be seen in Figure 29.

*Figure 29: Turbine with installed lever arm and weights for torque measurements.*

*Wind Tunnels Testing*

The primary wind tunnel used for testing is an open jet wind tunnel at the University of Maryland. The wind tunnel has a throat size of 30 inches by 30 inches and is capable of producing wind speeds up to 36 m/s. This wind tunnel was used for measuring cut-in speed, measuring the power curve, performing braking tests, and determining structural stability. A digital tachometer was used to monitor the turbine's rotational speed.


*Figure 30: Experimental setup.*

To measure the cut-in speed, the tunnel wind speed was gradually increased until the turbine began to spin. The starting wind speed was 3.18 m/s. This matches very closely with the aerodynamic predicted value of 3.2 m/s.

The power curve was found by measuring the voltage and current produced by the turbine as it was connected to the control electronics and load as it would be at the competition. The curve is shown in Figure 31. The turbine does produce power at low speeds starting at 3.2 m/s, but it is below 0.25 W until about 7 m/s. This low power is because the torque of the generator prevents the torque of the rotor from spinning up to its optimal tip speed.

After 7 m/s, the turbine begins to produce substantial power, and the relationship is fairly linear with wind speed. The energy in wind scales as a cubic function, but because of the rotor, generator, and load interaction, the power produced does not scale cubically. These interactions also explain why the rotational speed does not fit a nice curve. When the resistance changes to limit voltage, the torque of the generator increases so the rotational speed decreases. During the tests, the peak power was 16W, produced at 11 m/s. This value is lower than the reported rated power of the turbine. This discrepancy can partially be attributed to shortcomings of the testing wind tunnel used as the wind speed was measured at the centerline of the tunnel, but the wind velocity varied and decreased farther away from the center of the tunnel. One additional takeaway from the test, is that the turbine did reach its rated rotational speed at the rated wind speed meaning the generator and rotor design are well-matched.

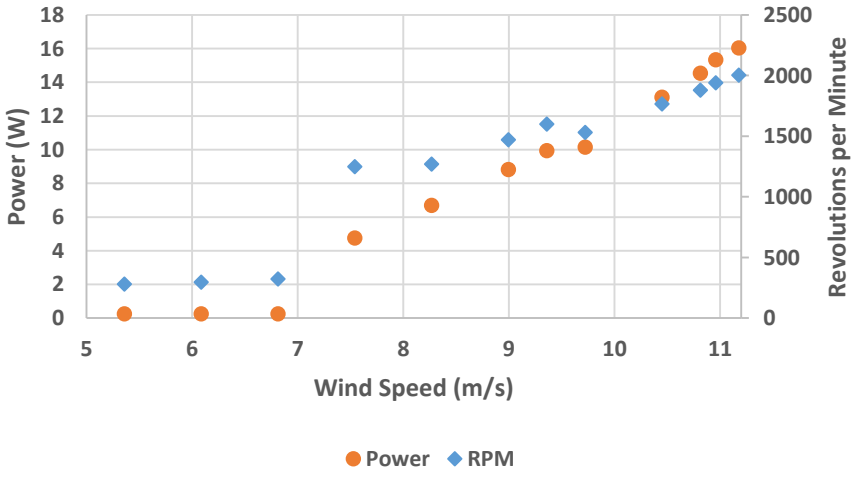


*Figure 31: Power curve data from testing.*

During the wind tunnel testing, the team also tested the frictional braking ability and ensured the structural integrity of various components. These tests indicated the brake would sufficiently stop the turbine and that all components were strong enough to withstand the forces of testing. Finally, the team also perturbed the turbine in yaw, and ensured that the turbine returned to the forward equilibrium. With these tests, the team is confident with the turbine's robust performance.

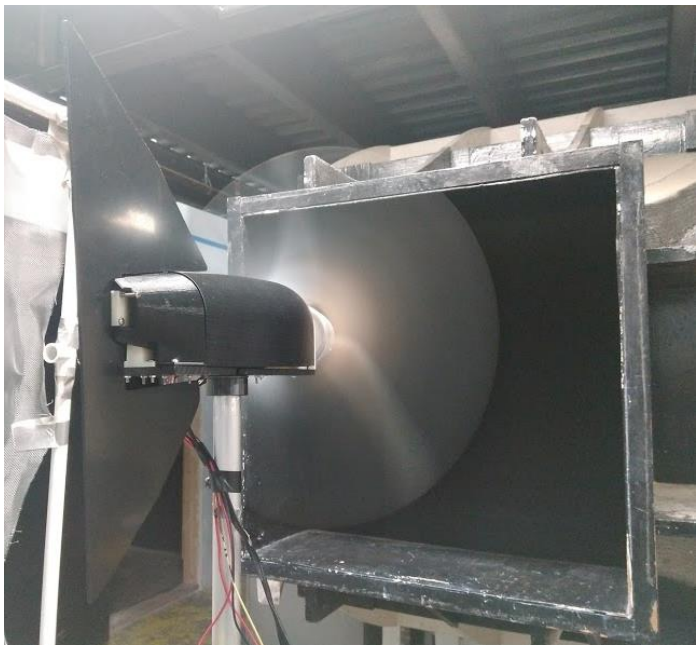

*Figure 32: The spinning turbine looking down the mouth of the wind tunnel.*

## References


1: University of Maryland Wind TERPines. *Technical Report.* 2016. Retrieved from https://energy.gov/sites/prod/files/2016/08/f33/UMD_REPORT_2016-05-01.pdf

2: Winslow, J., Otsuka, H., Govindarajan, B., and Chopra, I. *Basic Understanding of Airfoil Characteristics at Low Reynolds Numbers.* 7th AHS VTOL Unmanned Aircraft Systems and Autonomy Technical Meeting, 24-26 January 2017, Mesa, AZ.

3: Manwell, J. F., McGowan, J. G., & Rogers, A. L. *Wind Energy Explained: Theory, design and application.* Chichester, U.K.: Wiley, 2009.

4: Marten, D., Wendler, J., Pechlivanoglou, G., Nayeri, C. N., Paschereit, C. O. *QBlade: An Open Source Tool for Design and Simulation of Horizontal and Vertical Axis Wind Turbines.* International Journal of Emerging Technology and Advanced Engineering, Vol 3, 2013.

5: *PolyJet Materials Data Sheet*. Stratasys. Retrieved from http://global72.stratasys.com/~/media/Main/Files/Material_Spec_Sheets/MSS_PJ_PJMaterialsDataSheet.ashx

6: NREL Wind Prospector. Retrieved from https://maps.nrel.gov/wind-prospector/

7: *Fatigue properties and endurance limits of stainless steels*. British Stainless Steel Association. Retrieved from http://www.bssa.org.uk/topics.php?article=104

8: *Aluminum 6061-T6.* MatWeb: Material Property Data. Retrieved from http://www.matweb.com/search/datasheet_print.aspx?matguid=1b8c06d0ca7c456694c7777d9e10be5b


## Nomenclature

| | | | |
|---|---|---|---|
| $\alpha$ | Angle of attack | $k$ | Spring constant |
| $\zeta$ | Damping constant | $l1$ | Moment arm from tail lift |
| $\lambda$ | Tip speed ratio | $l2$ | Moment arm from thrust |
| $\mu$ | Coefficient of friction | $L$ | Lift |
| $\rho$ | Air density | $m$ | Mass |
| $\boldsymbol{\tau}$ | Shear stress | $M$ | Moment |
| $\omega$ | Rotational speed | N | Normal force |
| $A$ | Area | $P$ | Power |
| $C_L$ | Coefficient of lift | $R$ or $r$ | Radius |
| $C_P$ | Coefficient of power | $t$ | Time |
| $C_T$ | Coefficient of thrust | $T$ | Torque or thrust |
| $E$ | Bending stiffness | $S$ | Planform area |
| $F$ | Force | $U$ or $u$ | Wind speed |
| $g$ | Gravity | $U_r$ | Reference wind speed |
| $I$ | Second moment of area | $z$ | Hub height |
| $I_m$ or $I_G$ | Mass moment of inertia | $z_r$ | Reference hub height |
| $J$ | Polar moment of inertia | | |